2-1
MIX

Laboratory for Atmospheric and Space Physics
University of Colorado, Boulder, Colorado 80302

Photopolarimetry Team

Outer Planets Mission Definition Phase

Final Report

August 1, 1971 to August 31, 1972

Contract No. NGR 06-003-184

Introduction

This grant was awarded to the Laboratory for Atmospheric and Space Physics to support the participation of Dr. Charles F. Lillie as a member of the NASA-formed Photopolarimetry Team for the definition phase of the Outer Planets Mission.

The Photopolarimetry Team was formed to identify the scientific objectives which can be attained with a photometer/polarimeter experiment aboard a spacecraft which flies past the outer planets, and to determine the optimum design for this experiment. The team also was to provide scientific support for the Outer Planets Mission Science Steering Group.

The scientific objectives for this experiment were to be developed by the entire team, while the instrument design effort was divided between two groups of engineers: one at LASP, the other at the Santa Barbara Research Corporation (SBRC). SBRC would do the optical design and study detectors, while LASP would perform the mechanical and electrical design studies. In addition, certain special studies would be undertaken as specified by the science team.

LASP's work under this grant can be divided into three phases, a logical result of the evolution of the outer planets mission during the definition phase. During the first six months, Phase I, we developed a conceptual design, modifying it as the spacecraft design evolved. The instrument which resulted from this study was presented in our semi-annual report as appendix 1.

During the next two months, Phase II, we continued to refine this design and delve more deeply into the mechanisms for the aperture plate and filter wheel assemblies. We breadboarded the optical design, and we studied the effect of the trapped radiation environment of Jupiter on photomultiplier detectors. A revised optimum design for the photopolarimeter was developed during Phase II.

Phase III began when the Outer Planets Mission was revised to the concept of a Mariner-Jupiter-Saturn Mission. At the same time the Photopolarimeter Team was reorganized under a new team leader, and the decision was made to carry out sky background/zodiacal light measurements with one of the telescopes of the Meteoroid Detection Team. This involved the transfer of the LASP group to the other

team. During Phase III, therefore, the LASP engineering group developed a design for a photopolarimetry experiment using one of the 8-inch, F/1.1 telescopes of the Meteoroid Detection Team's "Sisyphus" experiment.

The work done by this laboratory during Phase I was presented in our semi-annual report and will not be discussed further. This report consists of three sections in which we present: (1) A discussion of the scientific objectives which can be attained with a photometer/polarimeter experiment; (2) Summaries of the special studies which were performed for the Photopolarimetry Team; and (3) A description of the photometer/polarimeter design which was developed for the Meteoroid Detection Team.

I. Scientific Objectives

In this section we summarize the scientific objectives of a photopolarimetry experiment for the Outer Planets Mission and indicate the approach by which these objectives can be met. A more detailed discussion may be found in the "MJS Photometer-Polarimeter Team Report," dated May 1, 1972, which was submitted to NASA by the Photopolarimetry Team. The instrument referred to is described in section III.

A. Objectives

The primary objectives of this experiment may be divided into four categories:

1. Interplanetary Medium
   (a) Determine the size distribution and spatial distribution of interplanetary dust particles;
   (b) Determine the probable composition of particles in the interplanetary medium.
2. The Atmospheres of Jupiter and Saturn
   (a) Determine the molecular scale height and abundance of H_2 and other gases;
   (b) Determine the index of refraction and size distribution of aerosol particles; and

(c) Obtain temperature vs. altitude profiles for the upper atmosphere.

3. The Satellites of Jupiter and Saturn

(a) Measure or set upper limits on the density of their atmospheres;

(b) Detect the presence of aerosols in their atmospheres; and

(c) Determine the texture and composition of their surfaces.

4. Saturn's Rings

(a) Determine the size and spatial distribution of particles in the various rings; and

(b) Discriminate between possible compositions for the ring particles.

Our secondary objectives include providing a backup imaging capability and a 2% photometric calibration for TV; providing a means of tying together the photometric calibrations of other instruments such as UVS and TV whose bandpasses overlap one or more of ours, and monitoring the radiation environment around the spacecraft through our photomultiplier dark current.

B. Approach

In order to meet the objectives of this experiment, we plan to use the instrument in two basic modes: as a photometer to study the temperature and number density distribution of gases in the atmospheres of Jupiter, Saturn, and their satellites, and as a polarimeter to study particulate matter in the interplanetary medium, in the atmospheres of the planets and their satellites and the rings of Saturn, and on the surface of the satellites.

1. Photometric Mode Experiments

(a) Stellar Occultations

On the basis of preliminary trajectory data for the MJS 1977 Mission, it appears there will be several opportunities to observe the occultation of bright stars by Jupiter, Saturn, and Saturn's rings. For example: Jupiter occults α Leo and α Vir with its dark limb; Saturn occults α Boo, εUMa, and η UMa; and α Lyr is occulted by Saturn's rings.

(1) Atmospheric Composition

At wavelengths where there are strong atmospheric absorption features, these occultations offer us the opportunity to use a technique based on the prin-

ciples of classical absorption spectroscopy to determine the number density of the absorbing species in the upper atmospheres of Jupiter and Saturn. At wavelengths where there is no important absorption, these occultations permit a determination of the refractive scale height (~temperature) of the planets' upper atmospheres.

The mathermatical inversion techniques which are used to recover atmospheric properties at the tangent point from occultation data have been described in detail by Hays and Roble (1968).

Ground-based measurements of stellar occultations have been used by Baum and Code (1952) and Evans and Hubbard (1971) to determine the variation in refractive scale height (temperature) with altitude in Jupiter's upper atmosphere (and to set severe limits on the atmospheric density of Io). Hays, Roble, and Shah (1971) have used stellar occultation data from the ultraviolet photometers on OAO-2 to determine the number density distributions of molecular oxygen and ozone in the earth's upper atmosphere. We plan to use the same techniques to determine the number density distributions of methane, ammonia, and molecular hydrogen and the

temperature profile in the atmospheres of Jupiter, Saturn, and their satellites which have atmospheres. The experiment is performed by setting the aperture wheel to the 0°.25 open field stop and the filter wheel to the filter which isolates the spectral region where a strong absorption feature occurs for the molecular species being studied. The photopolarimeter is pointed to the star which is to be occulted and the brightness of the star is measured 64 times a second for about 60 seconds. The data rate during this interval is 1280 bits/second. By averaging over several samples, a photometric accuracy of 1% can be achieved with 4th magnitude A stars. Table 3 indicates the count rate expected for α Lyr and α Vir for each molecular species:

TABLE 3

Stellar Occultation Experiment

Effective Wavelength	Feature	Counts/Sample	
		Vega	Spica
2200 Å	NH_3 absorption edge	16,485	82,031
2550	H_2 continuum	20,748	80,028
4000	ground-based comparison	52,888	39,878
6750	Rayleigh and aerosol scattering	3,204	1,807
7270	CH_4 absorption band	2,635	1,465

(2) Saturn's Rings

Stellar occultation measurements may also be used to study the material in Saturn's rings. Measurements with different filters will yield optical thicknesses at seven wavelengths between 2200 and 7300 Å. The spectral variation in the optical thickness (extinction) will yield the particle size if they are smaller than 10 μ. Occultation measurements made at different ring aspects as seen from the spacecraft will yield the ring thickness. High time resolution measurements of the occultation of a star by the rings will yield information on the particle size range above the Fresnel zone. At 5000 Å and 50,000 km the smallest detectable particle size is 5 meters. Particles as small as 20 m can be detected using the photopolarimeter and a 4th magnitude star.

(b) Terminator Scale Height

Measurements of the rate of decrease in intensity of light in the several wavelength bands will be made at the Jupiter and Saturn terminators. Similar measurements have been accomplished in the ultraviolet from the Mariner 9 spacecraft and give the scale height or temperature of the atmosphere as well as showing a

scattering layer as a secondary effect. The range of wavelengths chosen will provide temperature measurements at different pressure levels from 200 mb at the longer wavelengths up to 5 mb at the shortest wavelength. Ammonia condensate may be expected to occur in this pressure range, and its altitude and scattering properties may be expected to be measured accurately using photoelectric detection techniques. The proposed sampling rate will provide the opportunity to make a large number of measurements per factor of e reduction in intensity at the terminator. Using the 0°.25 aperature, the finite field of view can be deconvolved to give the gross temperature structure of the Jupiter and Saturn atmospheres at these major constituent pressure levels.

(c) Imaging Measurements

The photopolarimeter has the capability of producing low resolution images of Jupiter, Saturn, and Saturn's rings. Images can be produced at seven wavelengths between 2200 and 7270 Å by setting the aperature wheel to the 0°.25 clear aperature and rastering the photopolarimeter field of view across the planets either by slewing the platform or by rolling the spacecraft and

stepping the scan platform. Data would be readout 64 times a second (1280 bits/sec). A slew rate of 28 mr/sec would permit 10 readouts per field of view. The 0°.25 field of view would permit a resolution equal to the best ground-based observations (0".2) at 2 R_J or about 5 R_S. A considerable enhancement of the images could be achieved by deconvoluting the data with the instrumental profile of the photopolarimerer. Images produced with the photopolarimeter would have a photometric accuracy of about 1%. Images could also be produced using the polarizing filters to enhance planetary features such as cloud bands and the red spot of Jupiter. In addition to producing images at higher resolutions and shorter wavelengths than are possible with ground-based instruments, the photopolarimeter could observe from aspect angles unobtainable from earth.

Accurate photometric measurements of Saturn's rings obtained in this manner would be particularly useful to search for faint ring structure associated with the moons of Saturn. These observations would aid in discriminating between theories of the origin of the rings and mechanism by which the divisions in the rings are produced.

2. Polarimetric Mode Experiments

(a) Technique

Four Stokes' parameters, I, Q, U, and V, completely specify the state of polarization of a quasi-monochromatic wave. The advantages of measuring and using Stokes' parameters are: (1) They all have the same dimension of intensity; (2) They are additive and, therefore, most conveniently suited for analytical treatment; (3) From the Stokes' parameters we can generate the degree and plane of polarization and the ellipticity.

Wolstencroft and Rose (1967) observed that the degree of ellipticity, $e = V/I$, of the zodiacal light is of the order of 1%. Swedlund et al. (1972) found that the circular polarization of Jupiter and Saturn is very small ($e \approx 10^{-4}$). Consequently, measurements of V would probably not be worthwhile and will not be considered.

The plane of polarization of light, specified by the angle $\Psi = \frac{1}{2} \arctan (U/Q)$, singly scattered from Rayleigh particles is perpendicular to the scattering plane. Multiple scattering, scattering from aerosol particles (especially those of irregular shape), and reflection from surfaces can create odd orientations of the

plane of polarization. Therefore, measurements of U can give additional information on aerosol and surface properties and the importance of multiple scattering.

We propose to measure the total intensity, I, with no polarizer in the optical train. This is equivalent to the sum of two intensities measured by polarizers with their transmission axes at right angles to each other. For example,

$$I \equiv I(0°) + I(90°), \text{ or}$$
$$I \equiv I(45°) + I(135°).$$

The Stokes' parameter Q is equal to the difference between I and twice the intensity measured with a polarizer whose transmission axis is set at 90° from a reference plane,

$$Q = I - 2I(90°) = I(0°) + I(90°) - 2I(90°) = I(0°) - I(90°).$$

Likewise, U can be determined with one additional intensity measurement, I(135°),

$$U = I - 2I(135°) = I(45°) + I(135°) - 2I(135°) = I(45°) - I(135°).$$

B

So, with three intensity measurements (one without a polarizer and two with polarizers set at 90° and 135°), we can determine all three Stokes' parpmeters. The degree of polarization is generated as follows:

$$P = \sqrt{(Q^2 + U^2)}/I.$$

Such a system has the following advantages over a two-polarizer instrument: (1) It gives additional information on the plane of polarization; (2) When the plane of polarization of an incoming beam is at 45° to the axes of transmission of a two-polarizer instrument, it cannot determine whether the light is polarized or neutral. The system we propose can. The instrument will be calibrated in the laboratory prior to flight and the calibration will be maintained in-flight by observations of stars of known brightness and polarization.

In this manner we will be able to measure the degree of polarization at seven wavelengths with a precision of better than 1% and determine the plane of polarization to ±5°. With the phase angle coverage which can be obtained from the MJS spacecraft, we expect to

observe polarizations in the 10's of per cent, i.e.: 15-20% for atmospheric aerosols and up to 60% for Saturn's rings and satellite surfaces. We feel the accuracy we can achieve is adequate for an initial survey of the outer planets.

(b) Atmospheric Aerosols

Polarization measurements as a function of phase and wavelength yield information about the size and composition of particulate matter in the upper atmospheres of the planets. The large wavelength coverage of this instrument permits the contribution of Rayleigh scattering to be separated from that of particle scattering. The additional information contained in the polarization measurements permits a much more accurate separation of the different scattering components. Multiple scattering reduces the amplitude of polarization features, but does not change its sense, even at large ($\tau > 100$) optical depths. If the particles have a fairly regular shape, it is possible to fit theoretical models to the data and derive the index of refraction and particle size distribution, as has been done for Venus (Hansen and Arking, 1971).

During planetary encounter, we propose using this technique to study the various features observable on

Jupiter and Saturn in order to correlate particle size and probable composition with visible features.

(c) Satellite Atmospheres

Ingersol (1971) has used polarization measurements of Mercury and Mars at 200 Å resolution from 3200 to 7000 Å to set limits on their atmospheric density. With the large phase angle coverage we can achieve and short wavelength measurements to remove any particulate contribution to the polarization, it will be possible to detect a 10-meter atmosphere.

(d) Satellite Surfaces

Polarization measurements of the satellites of Jupiter and Saturn over a wide range of phase angles will permit us to characterize them according to their surface textures and probable compositions, i.e.: bare rock, dust covered, coated with frost. Figure 1 shows the polarization versus phase angle for three types of surfaces. Because the phase angles which can be obtained from earth are small (a maximum of 11° for Jupiter, 6° for Saturn), it has been necessary to obtain very precise measurements to discriminate between surface coatings. Measurements from the MJS spacecraft need not be so

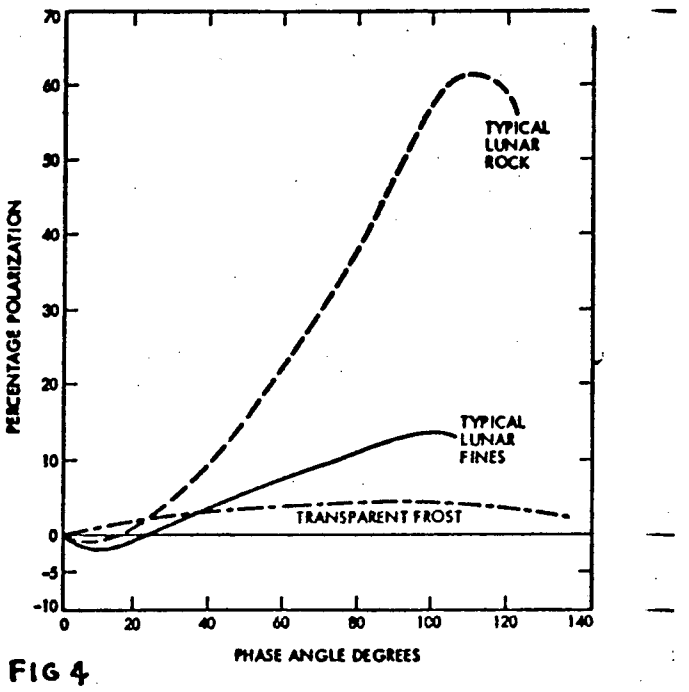

Figure 1

precise. Ground-based telescopic observations (Veverka, 1971) indicate that large differences are to be expected even among satellites of the same planet. These differences have important implications concerning their formation and subsequent evolution.

A geometric albedo can be determined in the 2200 - 7300 Å region for those satellites whose diameter can be determined by the imaging system. The geometric albedo of the satellites may also be determined from the slope of the polarization curve in the 20 - 60° phase angle region. For the moon and major asteroids, the polari-

zation slope is well-correlated with geometric albedo. Zellner (1971) has used this technique to find the albedo for Deimos which is in excellent agreement with results from Mariner 9.

(e) Zodiacal Light

During the planned spacecraft roll maneuvers of 0.5 AU intervals, the spectral distribution, intensity, and polarization of the zodiacal light will be mapped over the sky as close to the sun as possible (consistent with light shield length and with other scan platform instrument restrictions). This mapping will require that the scan platform be stepped at approximately 3° intervals on an axis perpendicular to the roll axis. Approximately 50 rolls are required for this purpose. To obtain a better determination of surface brightness of the sky as a function of solar distance and ecliptic longitude, the polarimeter should be pointed to a grid of selected areas of the sky once every week or two in addition to the full sky mapping at 0.5 AU intervals.

A similar telescope and other instruments currently being used to support Pioneer and Skylab operations will be used throughout the missions at the Dudley Night-Sky Observatory atop Mt. Haleakala in Hawaii. These

observations will uniquely determine the amount and optical properties of particulate light matter between the Earth and the spacecraft and, separately of particulate matter beyond the spacecraft. They will also aid in interpreting data from the flight instrument, and will measure temporal variations from the Pioneer, Skylab, and HELIOS data by serving as the intercalibration reference. Parallax measurements between the ground and spacecraft instruments can confirm or deny the existence of libration clouds and the so-called "bright blobs". In addition, near simultaneous ground and deep space measurements will aid in the interpretation of past and future ground-based astronomical measurements by directly determining sources and sinks of radiation, in the atmosphere, in the solar system, and beyond.

From these observations, maps will be produced of the starlight and the zodiacal light. The color of the zodiacal light will be studied as a function of solar distance and elongation and compared to the sun color (Peterson, 1967). The zodiacal light measurements can then be compared with models in the manner of Gillett (1966), Giese and Dziembowski (1967), and Wolstencroft and Rose (1967) to determine the spatial concentrations and properties of

the interplanetary particles. The zodiacal light is expected to be faint beyond Jupiter due to the reduced solar intensity. Measurements in the outer solar system will be extremely valuable in that they will provide the first sky measurements without a significant contribution from interplanetary particle scattering. Only under these unique conditions is it possible to separate integrated starlight and diffuse galactic light and to make possible a direct measurement of cosmic light.

The flight measurements at λ = 2500 and 2200 Å, which cannot be duplicated on the ground, are of particular interest because recent results from OAO-2 (Lillie, 1972) suggest that large numbers of very small particles may dominate the zodiacal light at short wavelengths. Information on the polarization and spatial distribution of these particles is crucial for determining their composition and origin.

References

Axel, L. (1972). Ap. J., 173, 541.

Baum, W. A., and Code, A. D. (1953). Astron. J., 58, 108.

Cook, A. F., Franklin, F. A., and Palluconi, F. D. (1971). NASA Technical Memorandum 33-988.

Evans, D. S., and Hubbard, W. B. (1971). Sky and Tel., 42, 337.

Hays, P. B., and Roble, R. G. (1968). J. Atmos. Sci., 25,1141.

Hays, P. B., Roble, R. G., and Shah, A. N. (1971). Scientific Results from the Orbiting Astronomical Observatory, ed. A. D. Code. NASA SP-000.

Ingersoll, A. P. (1971). Ap. J., 163, 121.

Margolis, J. S. (1971). Ap. J., 167, 553.

Price, M. J. (1970). ITT Research Institute Report, P-36.

Swedlund, J. B., Kemp, J. C., and Wolstencroft, R. D. (1972). Second Annual Meeting of American Astronomical Society, Division of Planetary Sciences, Kona, Hawaii.

Trafton, L. (1972). Ap. J., 175, 295.

Veverka, J. F. (1971). Icarus, 14, 355.

Wolstencroft, R. D., and Rose, L. J. (1967). Ap. J., 147, 271.

Zellner, B. (1972). Astron. J., 77, 183.

II. Special Studies

The following studies were undertaken to check critical design areas of the instrument described in our semi-annual report or at the request of the Photopolarimetry Team.

A. Radiation-Induced Dark Current in Photomultiplier Tubes

The photometers of the Wisconsin Experiment Package on OAO-2 (Code et al., 1970) responded to particles trapped in the earth's magnetic field in the same manner as photomultiplier tubes flown on previous spacecraft (Fowler et al., 1968). Eighty per cent of the time the dark current is constant at a level about 10 times higher than that observed on the ground prior to flight. When the spacecraft passes through the inner radiation belt, however, the dark current increases rapidly by three or four orders of magnitude above the nominal background level. Figure 2 is a map of the earth showing the subsatellite point of OAO-2 during orbit 7518 and the flux contours for trapped protons with energies greater than 3 MeV (Stassinopoulos, 1970). Figure 3 is a plot of dark current versus time for one of the WEP during the same time interval. The time at which each contour was crossed is indicated on the abscissa

of the diagram. The excellent correspondence between the proton flux level and the dark counts can be seen in Figure 4 where we plot dark counts versus proton flux. Similar plots can also be produced showing the correspondence between the flux of electrons and the dark current, since the electron flux contours generally parallel the proton flux contours in this region. Indeed, Fowler et al. (1968) attribute most of the dark current induced in their tubes to the effect of energetic electrons, although the OAO dark current variations seem to correlate most closely with the flux contours of protons.

The effect of trapped radiation on photomultiplier tubes of different types is shown in Figure 5. Here we plot the relative number of dark counts per unit particle flux for three of the WEP photometers versus the nominal dark current for each tube type. The tube types for which data are presented are listed in Table 1.

Two effects can be seen in Figure 2, a sharp increase and decrease in dark current as the spacecraft passes through the radiation belt and an induced dark current which decays exponentially with a time constant of about 20 minutes.

Dressler and Spitzer (1967) have studied the effect of 0.6 MeV electrons on EMR 541 photomultiplier tubes with various window-cathode combinations. They find events occur as a large pulse followed by a train of pulses. They suggest the train of pulses may be associated with direct excitation of electrons in the cathode by energetic electrons.

We may understand the OAO dark current measurements by assuming that energetic electrons and protons which are incident on the photomultiplier tube cathodes produce a large pulse immediately, followed by a string of pulses which resembles an enhanced thermal dark current component. The relative number of trailing pulses depends on the work function of the cathode as shown in Figure 5. After the spacecraft has passed through the radiation belt, many free electrons in the photomultiplier tube cathode are near the top of the "equipotential well" having been "excited" by incident particles. These electrons contribute to an enhanced thermal dark current which decays exponentially as they escape or radiatively decay.

A rule of thumb from the OAO data which can be applied to photomultiplier tubes on the Outer Planets Missions is

that one dark current pulse will be produced for every incident electron or proton per cm^2 with energies greater than 3 MeV from a bi-alkali photocathode. Cesium-iodide photocathodes produce a factor of seven fewer pulses. Thus, at 7.5 R_J we may anticipate a dark current of 6×10^4 counts/second from an EMR 541-N photomultiplier tube without special shielding or pulse-height discrimination or coincidence counting electronics according to the nominal model for the Jupiter Radiation Belt presented at the July, 1971, workshop at JPL.

REFERENCES

Code, A. D., Houck, T. E., Bless, R. C., McNall, J. F., and Lillie, C. F., 1970, "Ultraviolet Photometry from the Orbiting Astronomical Observatory. I. Instrumentation and Operation," Ap. J., 161, 377.

Dressler, K., and Spitzer, L., Jr., 1967, "Photomultiplier Tube Pulses Induced by γ Rays," Rev. Sci. Instr., 38, 436.

Fowler, W. B., Reed, E. I., and Blamont, J. E., 1968, "Effects of Energetic Particles on Photomultipliers In Earth Orbit up to 1500 km," NASA GSFC X-613-68-486.

Stassinopoulos, E. G., 1970, "World Maps of Constant B, L, and Flux Contours," NASA SP-3054.

Table 1

Photomultiplier Tube Data

Stellar Photometer No.	Tube Type	Cathode	Key Letter	Nominal Dark Current*	Relative Response
2	EMI 6256B	Bi-Alkali	N	2.5×10^{-11}	1.00
3	EMR 541-F	Cs-Te	F	2.0	0.75
4	EMR 541-G	CsI	G	0.3	0.14

*amperes at 20°C and 10^6 gain

Figure Captions

Figure 2 The subsatellite positions of OAO-2 during orbit 7518 (May 14, 1970) at 4-minute intervals plotted on a world map which shows the flux contours of protons with E > 3 MeV at an altitude of 800 km. (OAO-2 is in a circular orbit at an altitude of 776 km.)

Figure 3 The dark current from WEP Stellar Photometer No. 3 in digital counts per second versus time. The times at which the proton flux contours shown in Figure 1 were crossed are indicated for comparison.

Figure 4 The flux of protons (E > 3 MeV) predicted from the contours shown in Figure 2 (Stassinopoulos, 1970) versus net digital counts from the photomultiplier tube in WEP Stellar Photometer No. 3 during orbit 7518.

Figure 5 The relative sensitivity of three different cathodes to radiation induced dark current during orbit 7518 versus the nominal dark current (thermal) for that cathode type.

OAO-2 SUBSATELLITE POSITION vs. TIME (MIN)
ORBIT 7518 GMT 05:46:43 5/14/70

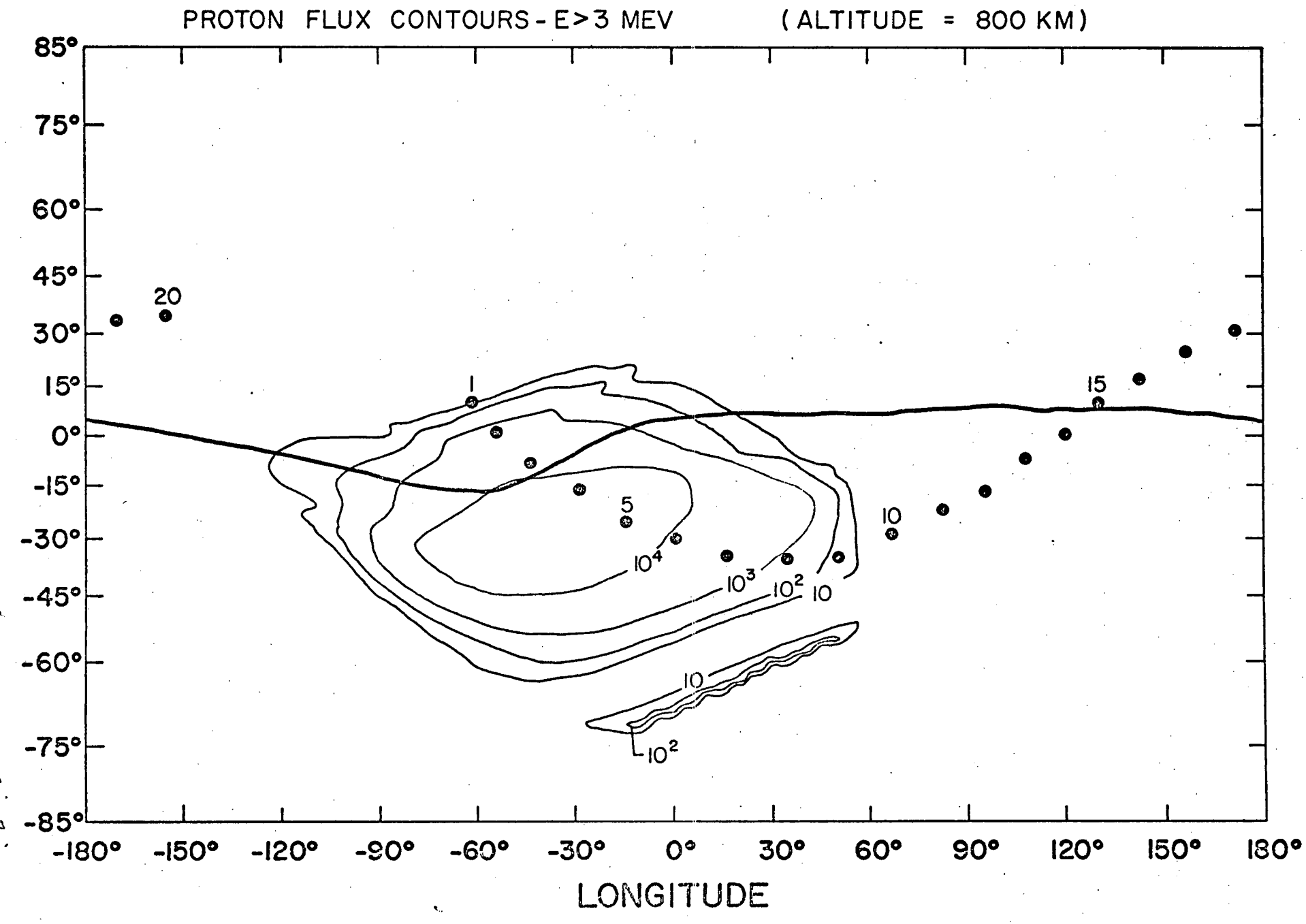

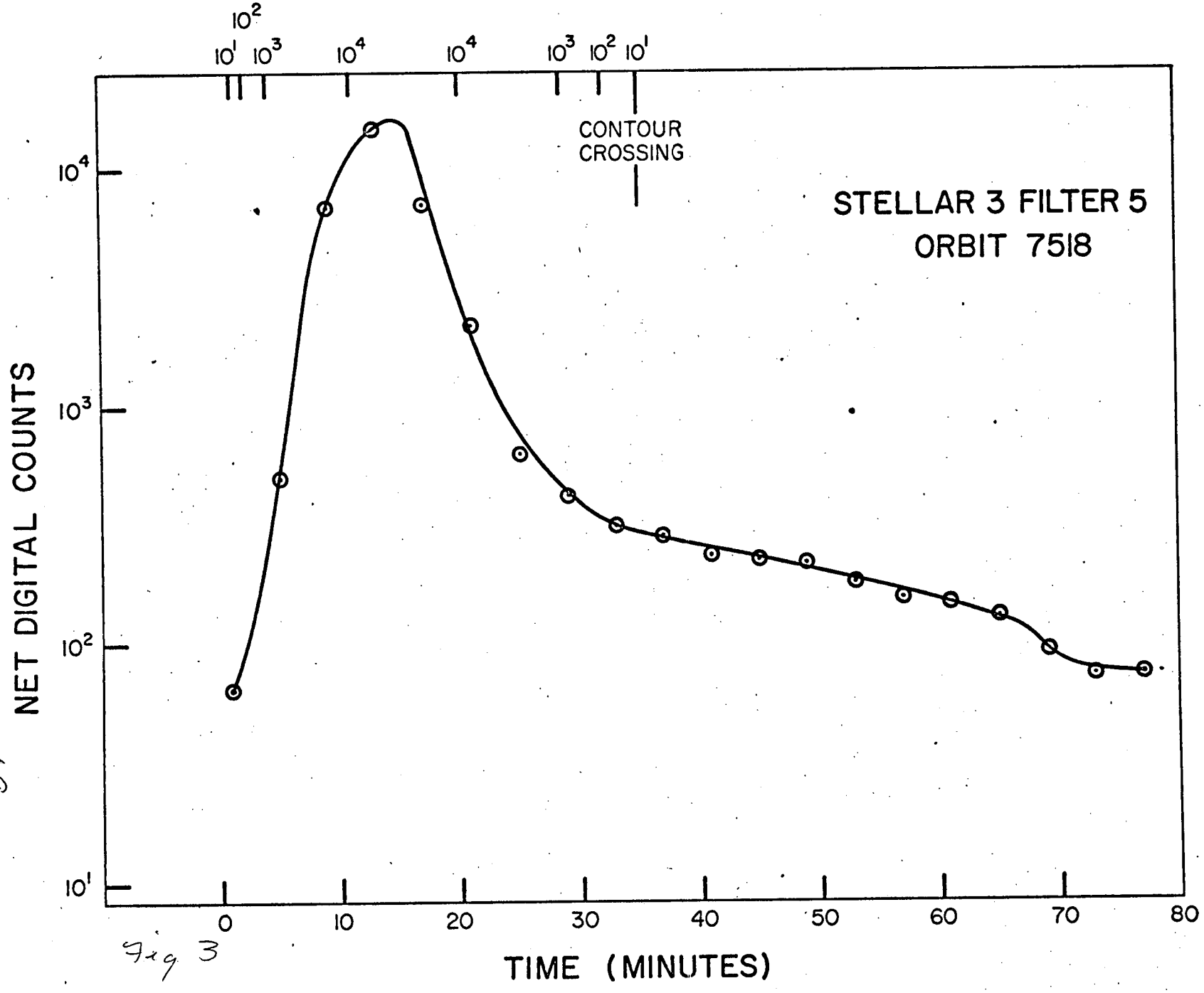
10^2
10^1 10^3 10^4 10^4 10^3 10^2 10^1
CONTOUR CROSSING
STELLAR 3 FILTER 5
ORBIT 7518
NET DIGITAL COUNTS
10^4
10^3
10^2
10^1
0 10 20 30 40 50 60 70 80
TIME (MINUTES)

Fig 3

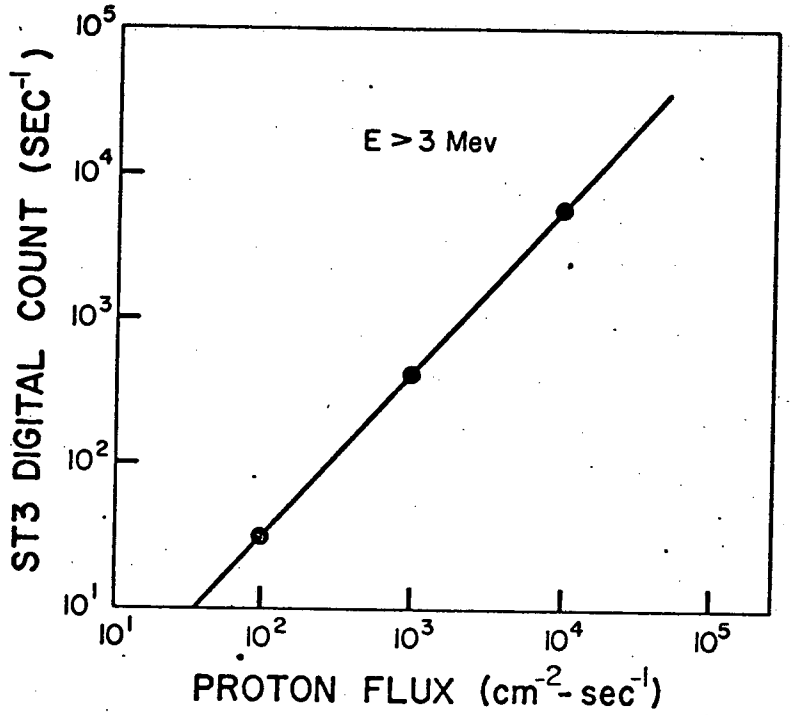
ST3 DIGITAL COUNT (SEC⁻¹)
E > 3 Mev
PROTON FLUX (cm⁻²-sec⁻¹)

Fig 4.

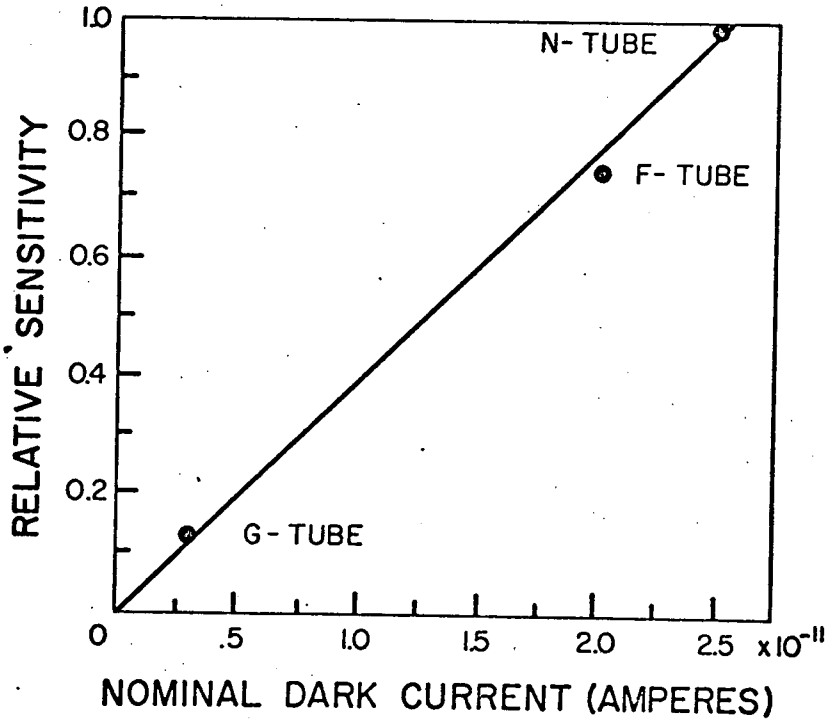
RELATIVE SENSITIVITY
N- TUBE
F- TUBE
G- TUBE
NOMINAL DARK CURRENT (AMPERES)
x10⁻¹¹

Fig 5

PRECEDING PAGE BLANK NOT FILMED

B. Evaluation of Photopolarimeter Instrument Deisgn

(1) Design Study Approach

The mechanical and electronic design of the photopolarimeter are dependent on the optical components and detectors chosen to meet the experiment objectives. In order to estimate power and weight requirements and provide recommendations on structural design, it is necessary to analyze the optical design. By studying several optical arrangements and their influence on weight and structural integrity, we can arrive at an optimum design for the instrument as a whole.

The starting point for all designs is the minimum experiment description, summarized briefly as follows:

1. Polarization measurements of 0.1% precision and photometry of 1% for planets.
2. Polarization and photometry measurements of precision of a few per cent for zodiacal light.
3. Measurements to be made in five passband ranges from approximately 2700 Å to 8200 Å.
4. Field stops to cover a range of acceptance cones from approximately 3° to 8 mr.

5. Minimum redundancy of measurement capability in the form of two photomultiplier channels.
6. Elliptical polarization will not be measured.
7. Aperture of light collection optics shall be at least 75 mm.

(2) Preliminary Layout

In order to record the low flux levels anticipated, photomultiplier tubes are required as detectors. To cover the required wavelength range, SBRC recommended the use of Ga-As photocathodes. Specifically, they evaluated the RCA Type C31025J photomultiplier, a moderately compact side-window tube, with a 0.25 x 0.5 inch cathode. The side-window configuration seems to offer packaging advantages over end-window tubes of equal size when two tubes are used in conjunction with a beam-splitting analyzer. SBRC also recommended a 75 mm F/4 Cassegrain objective for light collection. To determine both the magnitude and plane of polarization at each passband, measurements are performed at three different rotations of the plane of polarization of the incoming beam. For each passband, the filter wheel is provided with half-wave retarders oriented at 0°, 22.5°, and 45°.

The instrument described in this section incorporates these features. At the time the layout was prepared, final selection of the analyzer had not been made, so the size and positions of the analyzer, field lens, and Fabry lenses are approximate, as is the position of the photomultiplier tubes. Since the size of the components shown is typical of several types of prism analyzers, these approximations should not seriously affect the accuracy of the size and weight estimates. The weight estimates are fairly conservative, with items such as detectors, electronic parts, motors etc. based on presently available hardware, and fabricated parts, such as chassis plates, assumed to be machined from aluminum.

Optical layout affects the electronics in two ways. Larger optical components would require bigger photomultipliers and larger motor power supplies. Secondly, a more spread out optical system would tend to spread out the electronics with corresponding increases in harness weight. The system logic diagram will remain unaffected and apply equally well to any instrument meeting the minimum experiment requirements.

(3) Study of Relation of Optical Layout to Mechanical Design

(a) Selection of the Analyzer

With a 75 mm F/4 objective and a 3° field of view, the analyzer must have an acceptance angle of at least 17.2° over the entire wavelength range and a clear aperture of 15 mm diameter. A rectangular aperture of equivalent area should be acceptable. If both the P and S components of the polarized beam are to be measured, the analyzer must be some type of beamsplitter.

Polarizing beamsplitters fall into two basic categories: either thin film devices or birefringent crystal prisms. The preliminary layout assumed a thin film device, but thin film polarizers do not have sufficient acceptance angles or wavelength range for this application.

Of the various berefringent crystals, only calcite exhibits sufficient berefringence and transmittance over the wavelength range. Both the Glan-Thompson and Wollaston prisms have a sufficient acceptance angle, but the Glan-Thompson prism has a greater length than the Wollaston of the same

erally, the Glan-Thompson prism is not used as a beam-

splitter; instead the reflected component is absorbed by blackening the top of the prism, to avoid contamination of the transmitted component. The Wollaston prism causes both components to diverge symmetrically and both components are transmitted through the rear face, allowing four sides of the prism to be blackened. This combination of symmetry, acceptance angle and compactness gives the Wollaston prism a distinct advantage over the other styles.

Figure 6 shows a double Wollaston prism analyzer with apex angles of 40°, 80°, and 40°. Divergence of the two component beams is over 30° at 8200 Å.

(b) Matching the Objective to the Photocathode

A field lens is required to keep the beam diameter constant as it passes through the analyzer, and a Fabry lens is required to image the objective aperture on the photocathode at the correct magnification. Since the width of the photocathode is only about 7 mm, the photomultiplier tubes must be placed very close to the analyzer. With a 50 mm focal length field lens integral with the front face of the analyzer and a Fabry lens integral with the rear face, there is just sufficient optical path length to separate the beams and image the aperture on the photocathodes without severe overfilling.

Any increase in throughput for the system would require a tube with a larger cathode.

(c) Half Wave Retarders

Because of the cone angle of the beam and the bandpass of each set of filters, zero-order retarders must be used. For maximum accuracy, it is advisable to use achromatic retarders with a combination of crystal quartz and magnesium fluoride.

(d) Cassegrain Objective

The 75 mm F/4 objective recommended by SBRC is a good choice in that it is the largest objective that matches the proposed photocathode; the selection of a secondary magnification of 2.3 may not be optimum from the standpoint of sunshade design. For example, a magnification of 2 would allow a shorter sunshade extension to protect the opening of the primary baffle tube from direct radiation.

(4) Aperture Plate and Filter Wheel Study

(a) General Description

A d.c. torque motor will be used as a prime mover in both filter and aperture control systems. The torque motor for the return position filter wheel will

be a brush type motor with a wire wound armature and a permanent magnet starter. The limited rotation of the aperture sector allows the use of a brushless torque for the aperture control loop.

In each of the two control loops, the wiper of a multi-tapped potentiometer will be used to provide position feedback information. The potentiometer taps will be used in conjunction with the return control logic to provide positive position control.

Figure 7 is a sketch of the proposed mechanical configuration. The filter wheel motor and potentiometer are mounted on a single shaft with bearings at each end. In this manner, shaft alignment problems are eliminated, and system friction is minimal. Figure 7 illustrates standard ball bearings which may present lubrication problems during extended space travel. A pivot and jewel bearing as illustrated in Figure 8 should provide a lubrication-free rotation with a minimum amount of friction. As shown, the jewels are spring-mounted, and the shaft is designed to bottom out in both the radial and axial direction to protect the pivot to jewel from excessive shock loading.

(b) Filter Wheel Control

Figure 9 is a block diagram of the filter wheel control system. The seven tap potentiometer is excited with a D.C. voltage that also serves as a reference for the system's decoder and analog switch. The voltage wiper of the potentiometer is proportional to the angular position of the shaft and, hence, of the filter wheel. In operation, a control command signals the Up/Down counter to advance or retard its position. The output of the counter is decoded and used to activate FET analog switches that connect various potentiometer taps to the input of the system's summing amplifier. The output of the summing amplifier is proportional to the difference in voltage of the connected tap and the wiper of the potentiometer. This output signal then drives the potentiometer wiper directly to the position of the connected tap independent of the excitation voltage. By connecting two potentiometer taps simultaneously, the wiper can be drawn to a position midway between taps, thus providing a total of seventeen possible command positions.

Servo compensation is provided in the feedback loop of the summing amplifier. Compensation is necessary

since the system measures position and control torque which is in proportion to

To conserve power, a pulse width modulation system is used to drive the torque motor. This pulse width modulation system has built-in hysteresis and minimum width control to assure zero motor drive at the null position. Figure10 illustrates the pulse width system circuitry and includes a plot of input-output characteristics.

The system power amplifier is simply a four transistor bridge circuit as shown in Figure11. The armature of the torque motor can be tuned to reduce inductive transients.

(c) Torque Motor Selection

To select the drive system motor size, it will be necessary to calculate the system inertia, estimate the system friction, and decide upon an acceptable transition time from one filter position to the next.

In general,

$$(1) \qquad \Sigma T = I_s \frac{d^2\theta}{dt^2}$$

(2) $\tau_x - \tau_f = I_s \frac{dw}{dt}$

(3) $\frac{(\tau_x - \tau_f)t}{I_s} = \omega + \omega_0$ (ω_o, Angular Velocity at time to = 0)

(4) Since $\omega = \frac{d\theta}{dt}$, $\frac{(\tau_x - \tau_f)t^2}{2I_s} = \theta + \theta_0$

Using $\theta_{1-2} = 20°$ (one step of filter wheel).

Assume optimum control, i.e.: Max. + α from 0-10°

Max. - α from 10-20°.

(5) From (4), $t^2 = \frac{2I_s\theta}{\tau_x - \tau_f}$

(6) $t_{0-10°} = \frac{\sqrt{2I_s\theta_{10}}}{\tau_x - \tau_f}$

(7) or $t_{0-20°} = \frac{\sqrt{8I_s\theta_{10}}}{\tau_x - \tau_f}$

(8) $\tau_x - \tau_f = \frac{8I_s\theta_{10}}{t_{0-20}}$

Equation (7) specifies the optimum transition time for a given net torque ($T_x - T_f$). Conversely, Equation (8)

yields the motor size for an allowed transition time $T_{0\text{-}20°}$.

Using a standard "inland" 6-oz. in torque motor and a filter wheel configuration as illustrated in Figure 12, it is easy to calculate system inertia and, hence, the optimum transition time.

$$I_{motor} + I_{wheel} + I_{pot.} + I_{shaft} = I_{system}$$

$$I_{system} \quad .015 \text{ in oz sec}^2$$

$$T_{0\text{-}20°} = \frac{8(.015)(\frac{10}{57.3})}{.9(6)} = .02 \text{ seconds.}$$

This figure assumes optimum control and an estimated 0.6 oz in friction. The total weight of the motor, filter wheel, potentiometer, and pivot shaft is approximately five ounces.

(d) Aperture Control

A variable aperture sector is shown in Figure 7. The mechanical configuration of this control system is identical to that of the filter wheel system with the exception of the number of required potentiometer taps.

D.

The inertia of the variable aperture sector is only a fraction of that of the filter wheel and, hence, a smaller torque motor would be used to conserve weight and space.

III. Design of the Zodiacal Light Photopolarimeter for the ILIAD Experiment

A. General

In describing the photopolarimeter in the previous section, it was shown that the primary aperture and field of view were a maximum for the proposed photomultipliers. Because of the low radiance of zodiacal light, it would be very desirable to increase the aperture of the instrument. Therefore, a basically different design would be needed in order to obtain significantly greater throughput while remaining within the allocated power and weight limits.

Discussions with the Particulate Science Team suggested that the asteroid-meteroid detector photometers aboard Pioneer 10 could serve as the starting point for a large aperture photopolarimeter. The modified instrument is shown in Figure 13. The back focal length of the Cassegrain objective is increased so that the focal plane is at the aperture wheel behind the primary mirror. Absorption polarizers are used instead of a Wollaston analyzer, thereby allowing a much greater acceptance angle. This instrument uses a single photomultiplier with a

1.25-inch diameter cathode. With an 8-inch primary and a 4° field of view, this instrument will collect twelve times more radiation than the 3-inch - 3° instrument described previously.

Since the filter wheel no longer contains half-wave retarders, buy only filler substrates, this will result in weight reductions and reduced motor-power requirements. The use of a single photomultiplier channel and replica mirrors on aluminum substrates contribute even more substantial weight reductions.

Note that the modification of one of the photometer telescopes into a photopolarimeter does not interfere with its original function as a meteroid detector. It is intended that this instrument will operate primarily in the meteoroid detection mode, during cruise, and serve as the fourth detector in the time-of-flight experiment.

B. Instrument Design

The instrument (see Figure 13) is basically a large aperture, multi-purpose photometer. Light is collected by an 8-inch Ritchie-Chretien version of a Cassegrain telescope, whose specifications are listed in Table 2.

At the focal plane of the telescope there is an aperture/polarizer wheel which contains a dark position, a calibration source, three 4° field stops, and three 0°.25 field stops. For each aperture size there is a clear aperture and two apertures equipped with polarizers. The large aperture polarizers are oriented at 0° and 90° rotation. The small aperture polarizers are oriented at 90° and 135° rotation. Behind the aperture/polarizer wheel is a filter wheel containing seven medium-band interference filters and an open position. Both wheels are shown in Figure 14. Each wheel is driven by an 8-position stepper motor and can be driven to any position or run in any of several modes as shown in Table 3 using a 12-bit command.

The detector is a quartz-window, end-on photomultiplier tube with S-20 cathode response, located directly behind the filter wheel. The output signal at the anode provides analog data for meteoroid detection and pulse-count data for photopolarimetric measurements. The data rate can be high, medium or low: either 1280 BPS with the wheels held in one position; 20 BPS with the wheels cycling through a complete set of measurements (three

polarizer positions per filter, 7 filters); or a 20-bit word every 64 seconds with the sheels cycling or stationary. Gain changes to handle the large dynamic range of light levels to be measured ($\sim 10^6$) is accomplished by varying the high voltage to the photomultiplier tube. A data word consists of a 14-bit (15 bits known) compressed data readout, 4 bits for filter and aperture wheel positions, one bit overflow time flag, and one bit spare.

Telescope design and construction will be the same as the meteorite detector telescope on Pioneer 10 and G. The photomultiplier tube will be the same as on Pioneer 10 and G. The four UV filters will be equivalent to those on OAO-2 and the three filters for the visible and near IR will be equivalent to those on Skylab. Stepper motors will be of the type used on OSO-I and similar to Mariner 9 construction. The high and low voltage circuit design is similar to that used for Atmospheric Explorer.

Table 2

INSTRUMENT CHARACTERISTICS

1. General

(a)	Weight	3.51 lbs.
(b)	Power	1.30 watts, max., 0.68 watts, ave.
(c)	Volume	935 in.^{3} (including sunshade)
(d)	Location	Scan Platform (bore-sighted w/TV)
(e)	PMT Cathode	S-20 or ERMA
(f)	Polarizer	Polacoat on fused silica
(g)	Operating Temp.	-150 °C ± 35 °C
(h)	Temp. Control	Passive, 0.7 w heater when off

2. Optics (Ritchie-Chretien, Cassegrain Telescope)

(a)	Primary	8-inch diameter, F. 1.0
(b)	Secondary Magnification	1.1
(c)	Vertex Spacing	4 inches
(d)	Field of View	4° total defined by focal plane field stop

3. Filter Bandpasses

Position No.	Nominal Wavelength	Half-power Bandpass	$1/\lambda$
1	2100 Å	300 Å	4.8 μ^{-1}
2	2500	300	4.0
3	2900	300	3.4
4	3300	200	3.0
5	4200	100	2.4
6	5300	100	1.9
7	7200	200	1.4
8*	5000	~6500	-

*Open window for meteoroid detection

4. Aperture Ensemble (Eight Positions)
   (a) Two field stops of 4° equipped with orthogonally oriented polarizers
   (b) Two field stops of 0.25° equipped with orthogonally oriented polarizers
   (c) Two open apertures of 4° and 0.25°, respectively
   (d) One dark position
   (e) One calibration position

5. Drive
   (a) Eight position stepper motor for filter wheel
   (b) Eight position stepper motor for aperture wheel

Table 3

INSTRUMENT CONFIGURATIONS

1.	Instrument power	ON or OFF
2.	Spacecraft/Instrument data rate	20 BPS or 20 bits/64sec
3.	Instrument integration time	1 sec or 64 sec
4.	Instrument mode commands	(12 bit word)
	a. Filter wheel	
	1. index to any one of 8 positions	3 bits
	2. run or inhibit	1 bit
	b. Aperture wheel	
	1. index to any one of 8 positions	3 bits
	2. run or inhibit	1 bit
	3. toggle between 2 polarized positions	1 bit
	4. low rate or high rate integration	1 bit
	5. high voltage OFF	1 bit
	6. spare	1 bit

5. Data
   a. High rate: 20 BPS with 2 readings per position of filter or aperture wheel
   b. Low rate: 20 bit word every 64 sec with two readings per position of filter or aperture wheel
   c. Cruise
      1. Meteoroid mode and roll mode -- low rate
      2. Pointed mode -- high rate
   d. Encounter -- high rate
   e. Data word
      1. PMT data, 20 bit counter (1,048,576 pulses)
      2. Data compression, 20 bit shift register and 5 bit counter
      3. Data readout, 14 bits (15 bits known), 4 bits filter wheel and aperture wheel positions, 1 bit overflow time flag, 1 bit spare
6. Analog Engineering Data
   a. LVPS monitor, 0 to 3V
   b. HVPS monitor, 0 to 3V
   c. Temp. optics monitor 0 to 3V
   d. Temp. electronics monitor 0 to 3V
   e. Solar sensor monitor 0 to 3V

Table 4

Weight and Power Estimate

Power Estimate	
PMT	.025 W
Pre-amps	.125 W
HVPS	.100 W
Housekeeping	.050 W
Misc.	.100 W
Logic	.050 W
LVPS (no motor running)	.225 W
Total (no motor running)	.675 W
LVPS (with motor)	.850 W
Total (with motor)	1.300 W
Weight Estimate	
Mechanical/Optical	
Light baffle - sunshade	0.35 lb.
Primary mirror	0.45 lb.
Secondary mirror	0.08 lb.
Chassis plate	0.43 lb.
Secondary support with Cassegrain baffle	0.10 lb.
Filter wheel	0.08 lb.
Aperture wheel	0.07 lb.
Filter wheel motor	0.15 lb.
Aperture wheel motor	0.13 lb.
Cover	0.12 lb.
Misc.	0.25 lb.
Total Mechanical/Optical	2.21 lb.
Electronics	
PMT assembly	0.23 lb.
Pre-amps	0.09 lb.
HVPS	0.09 lb.
Harness	0.22 lb.
Misc.	0.07 lb.
LVPS	0.27 lb.
Logic	0.33 lb.
Total Electronics	1.30 lb.
Total Instrument	3.51 lb.

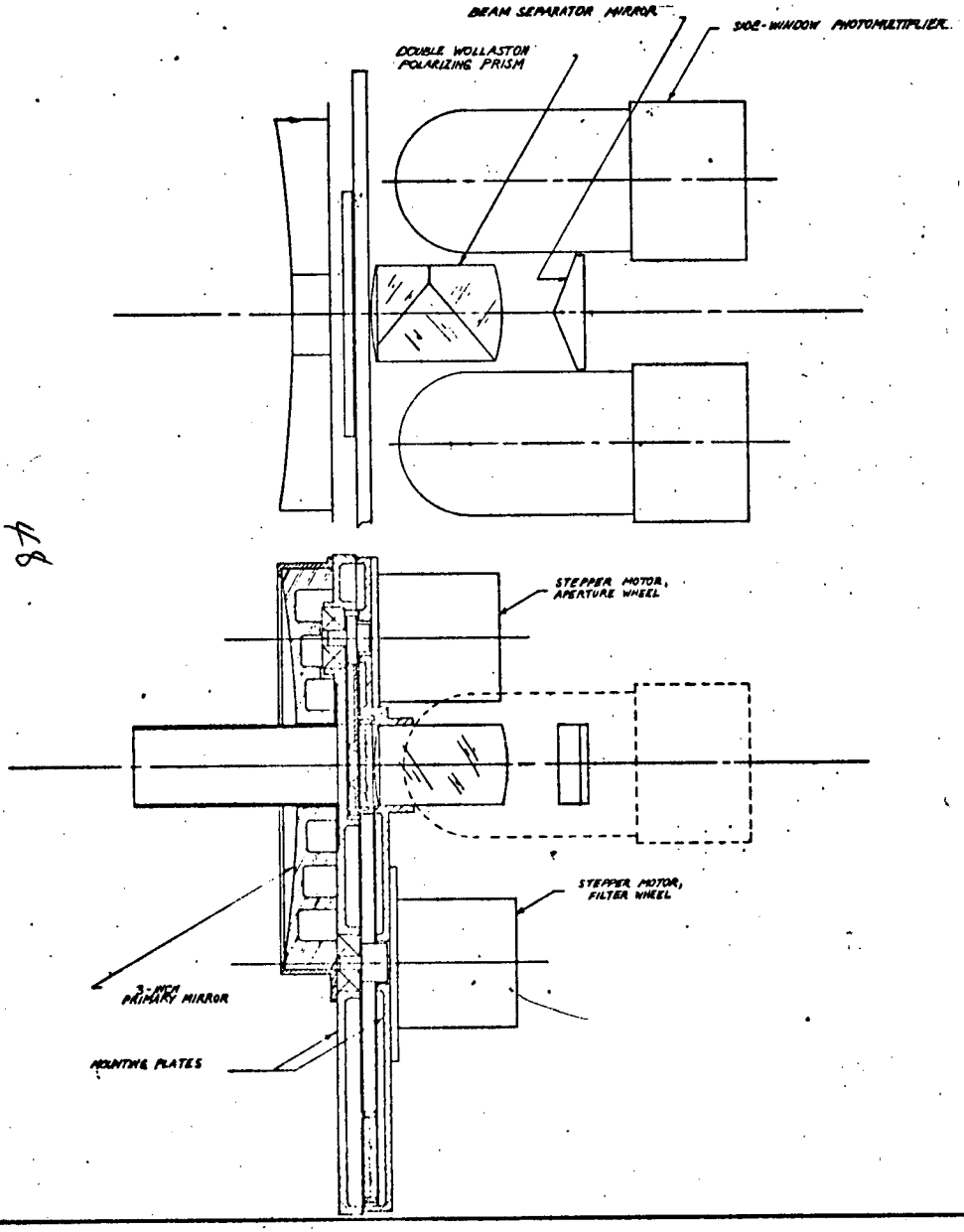

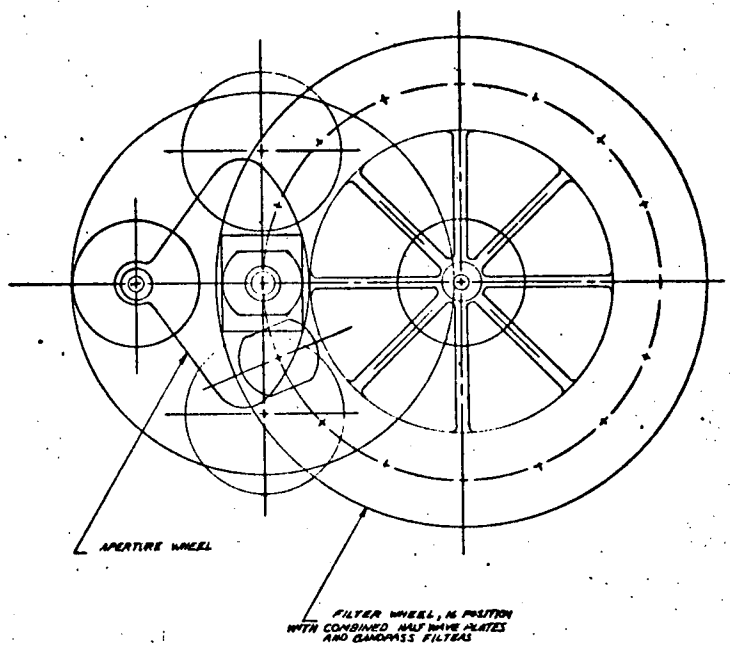

REVISIONS

ITEM NO	NO REQD	PART OR IDENTIFYING NO	PART NAME	STOCK SIZE OR DIMENSIONS	MATERIAL

BILL OF MATERIAL

UNLESS OTHERWISE SPECIFIED
DIMENSIONS ARE IN INCHES
MILLIMETERS ARE IN PARENTHESIS
TOLERANCES: .XXXX BASIC
.XXX ± .005 (.13)
.XX ± .02 (.51)
ANGLES ± 0° 30'
Metric Equivalents, to the nearest .01 mm, are Given For General Information Only and Are Based Upon 1 Inch Equals 25.4 mm.
DO NOT SCALE DRAWING
REMOVE BURRS & SHARP EDGES
MACHINE FINISH

CONTRACT NO
DRAWN 1-13
CHECKED
APPROVED
APPROVED

DEPARTMENT OF ASTRO-GEOPHYSICS
UNIVERSITY OF COLORADO
BOULDER

POLARIMETER CONCEPT

SIZE D
CODE IDENT NO 28981
SCALE
SHEET

APPLICABLE SPECIFICATIONS

NEXT ASSY | USED ON
APPLICATIONS

Fig 6

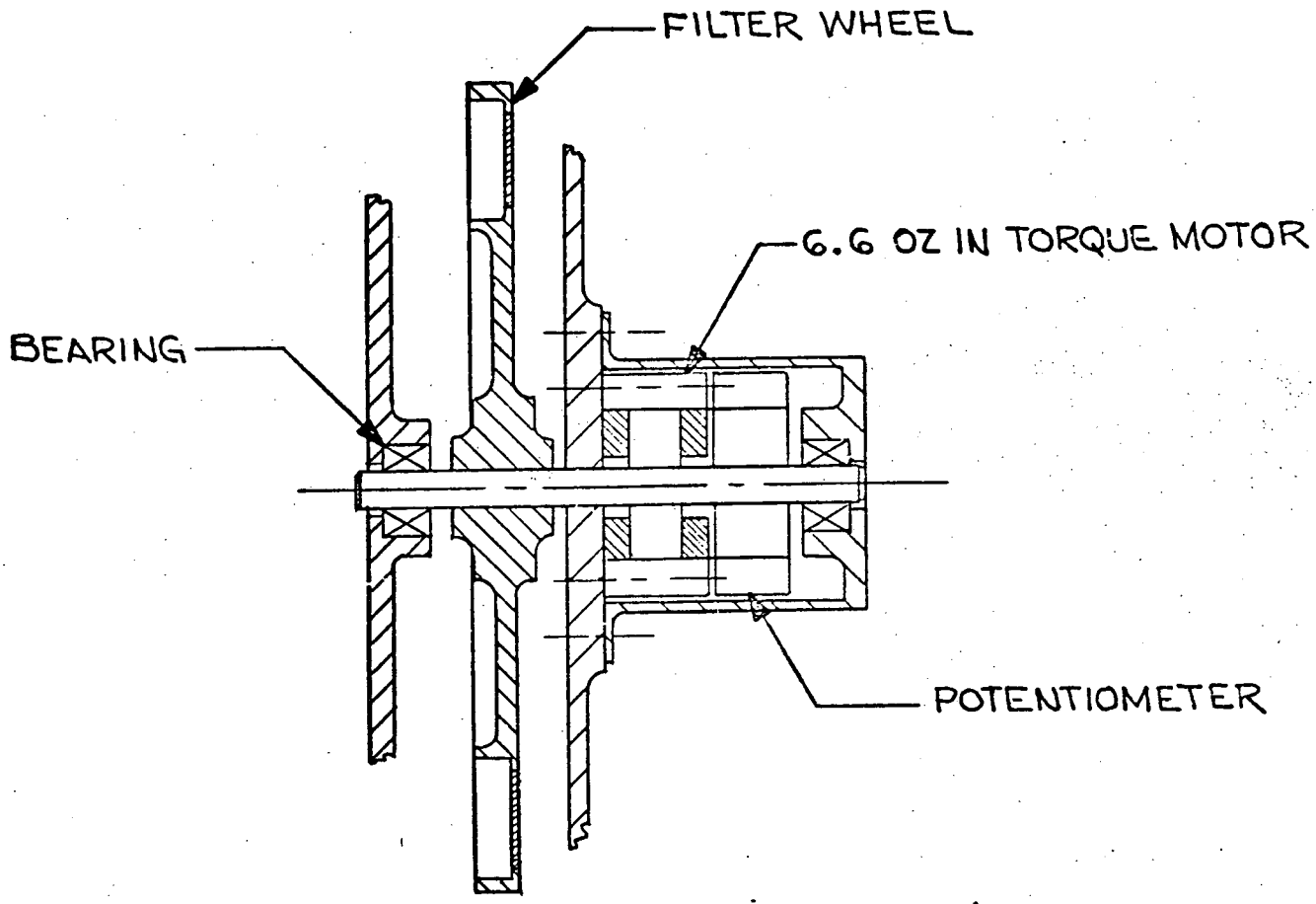

FIGURE 7

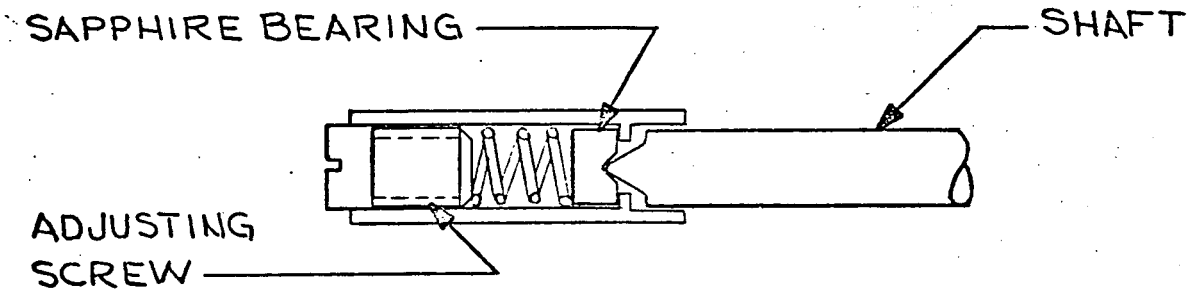

ENLARGED VIEW OF
OPTIONAL BEARING

FIGURE 8

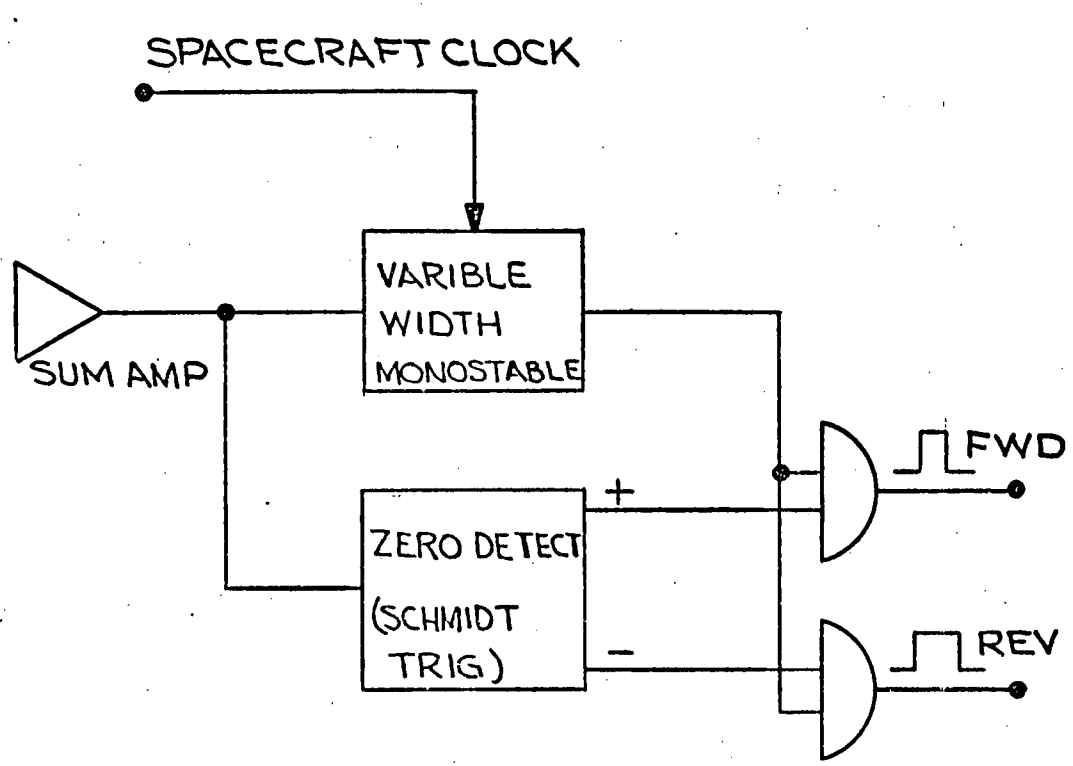

CIRCUIT

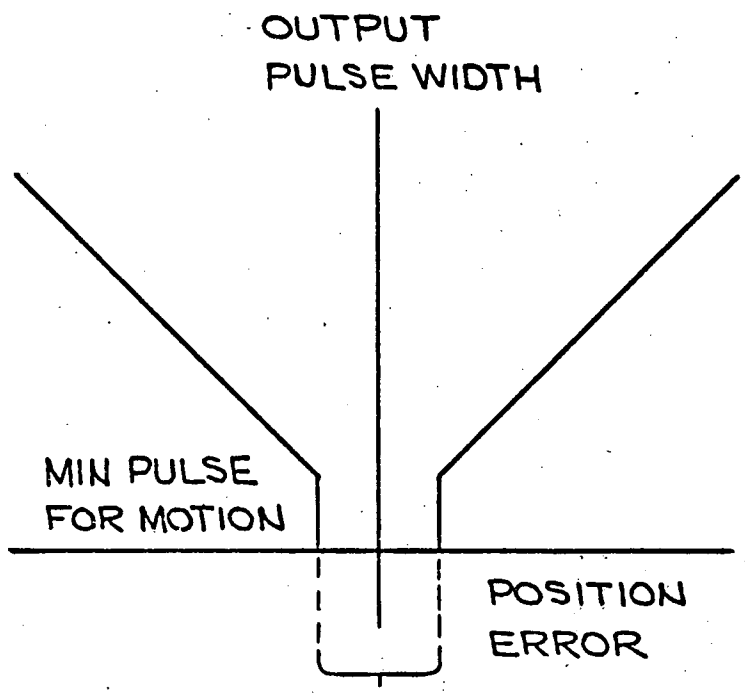

TRANSFER CHARACTERISTICS

PULSE WIDTH MODULATION SYSTEM

FIGURE 9

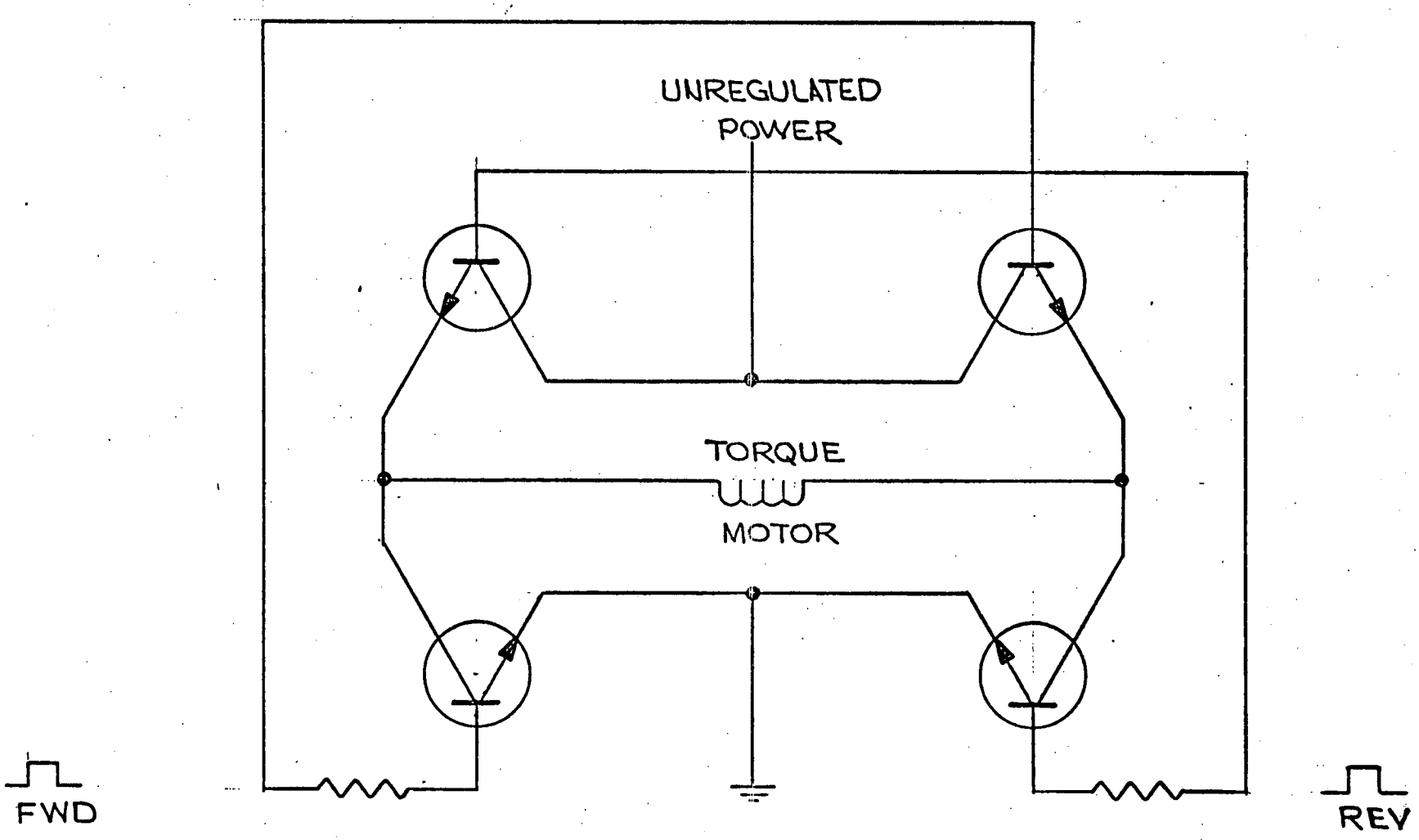

POWER AMPLIFIER

FIGURE 10

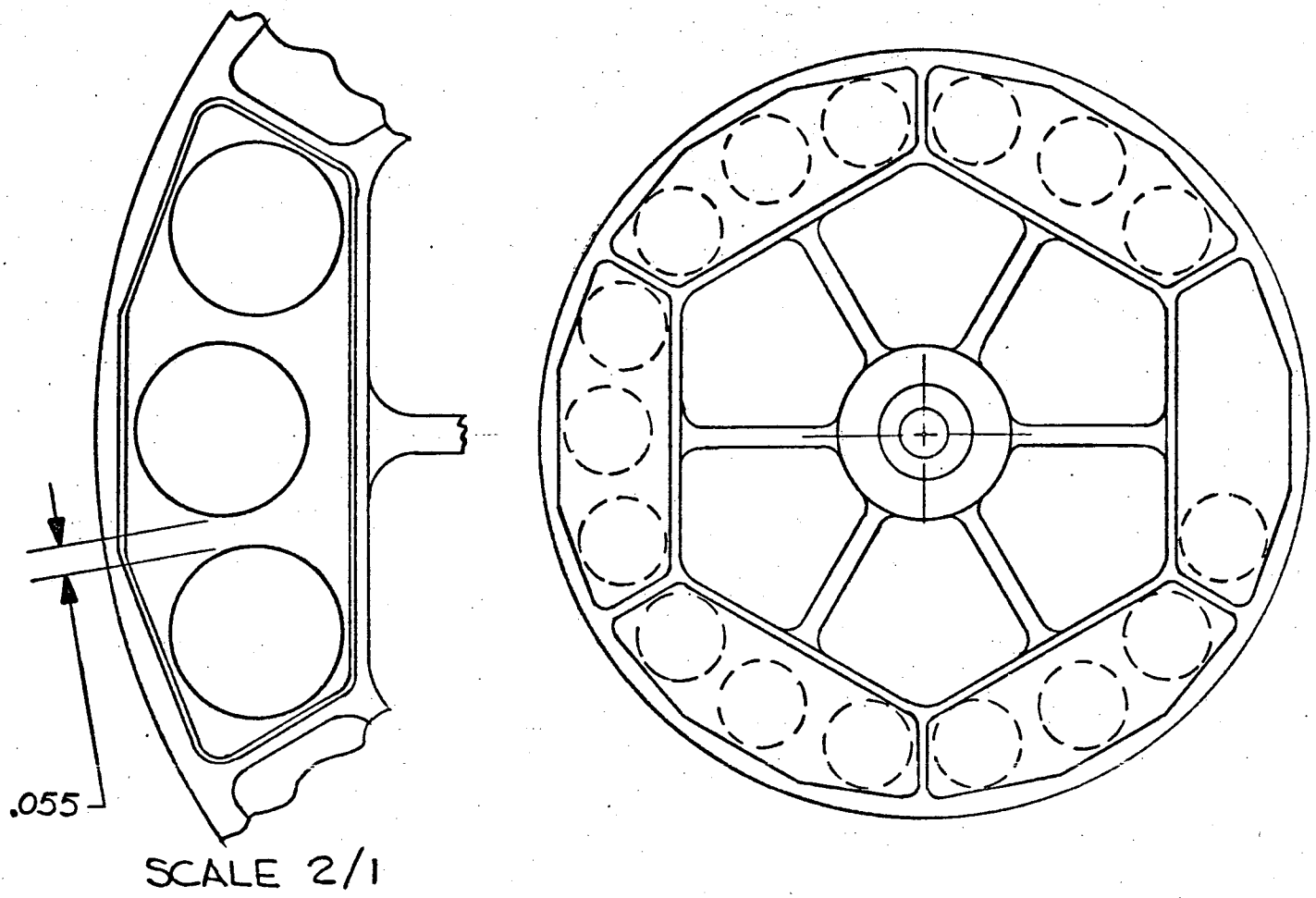

SCALE 2/1

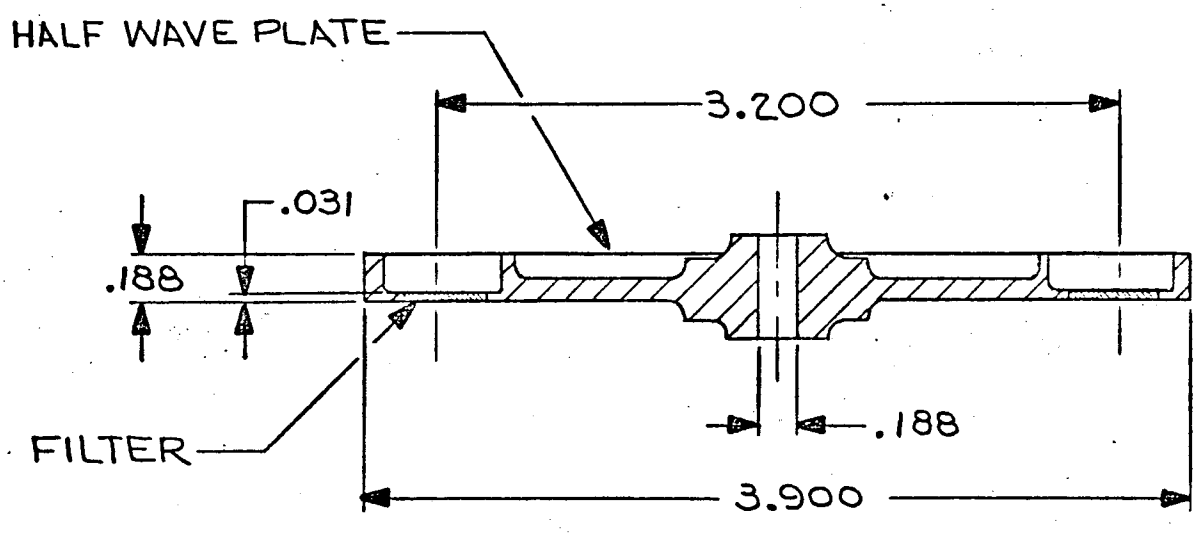

MATL - BERYLLIUM
SCALE 1/1

FIGURE 11

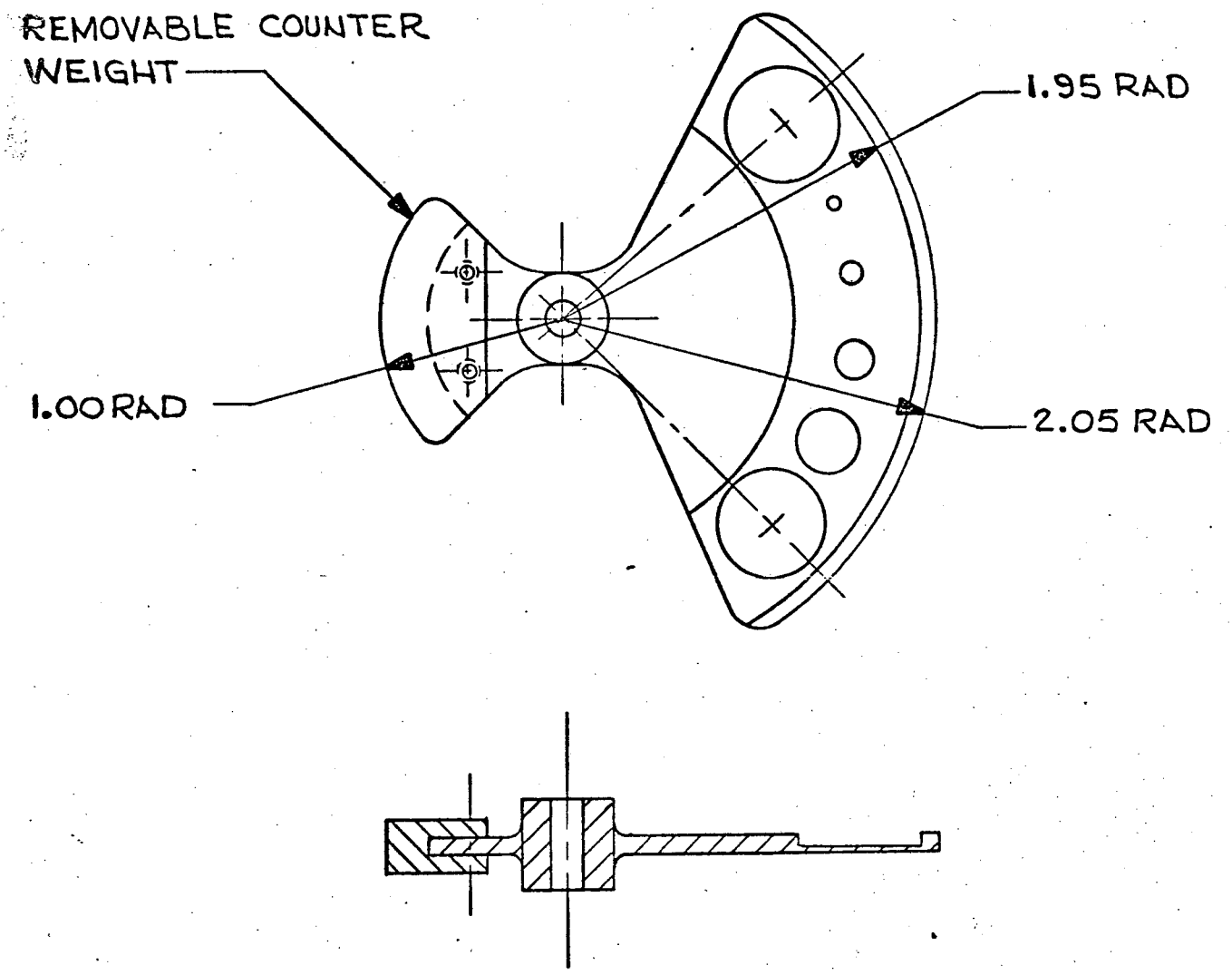

MATL - BERYLLIUM
SCALE 1/1

FIGURE 12

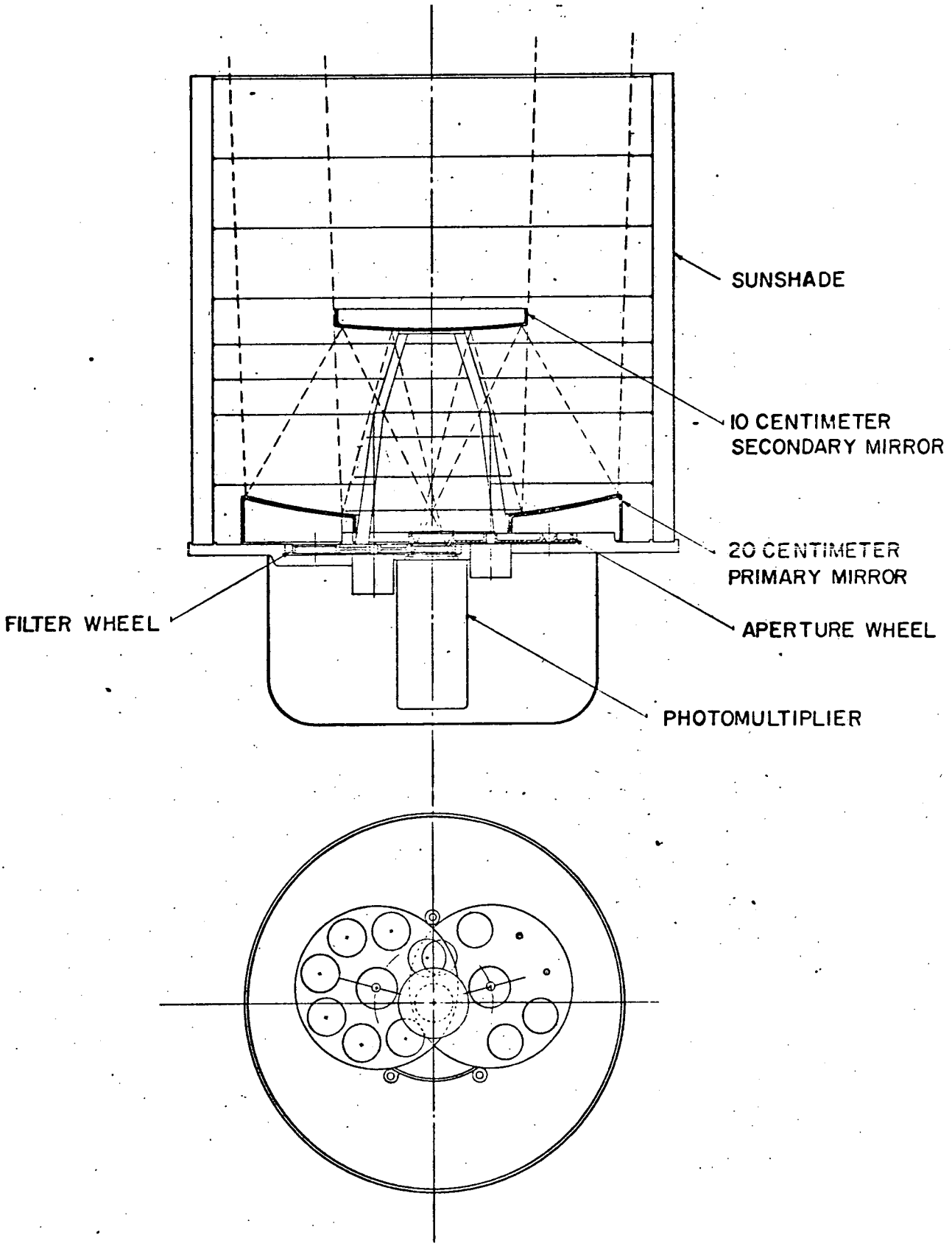

PHOTOPOLARIMETER
OPTICS AND FILTER WHEEL

FIGURE 13

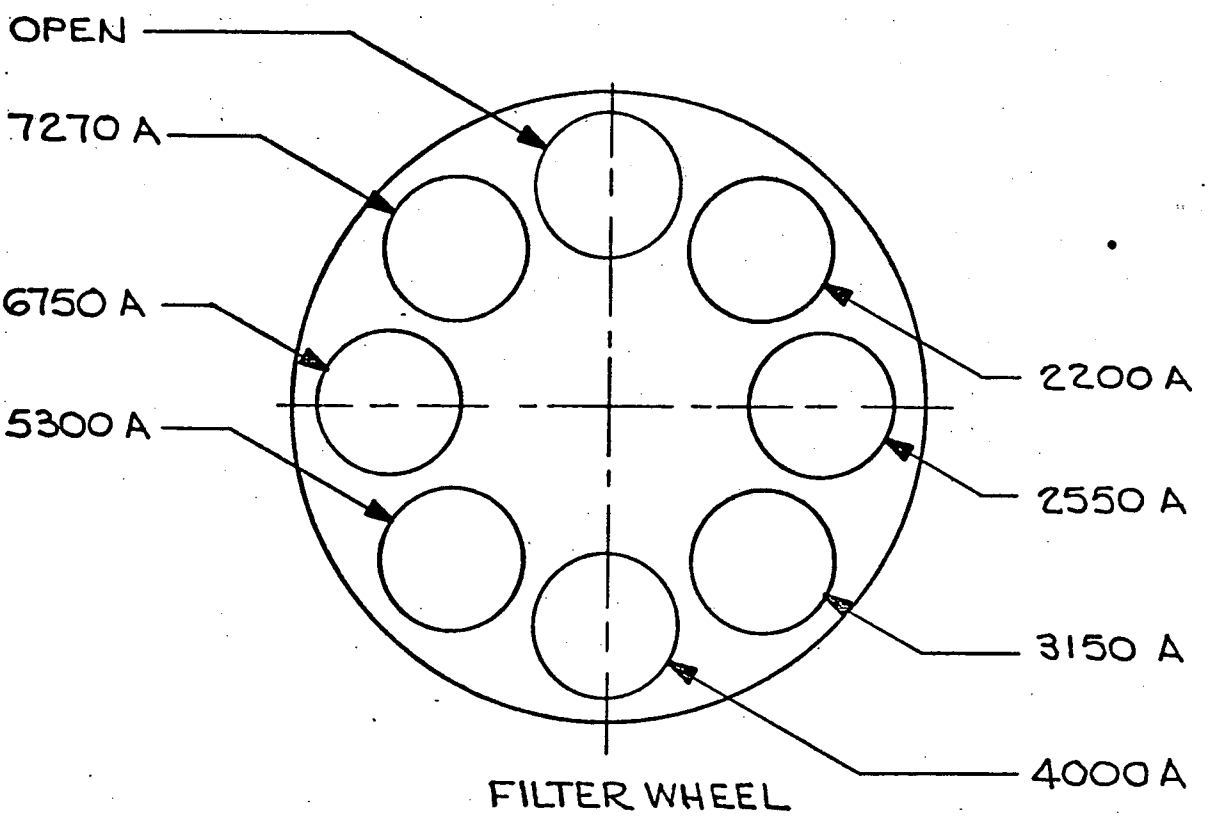

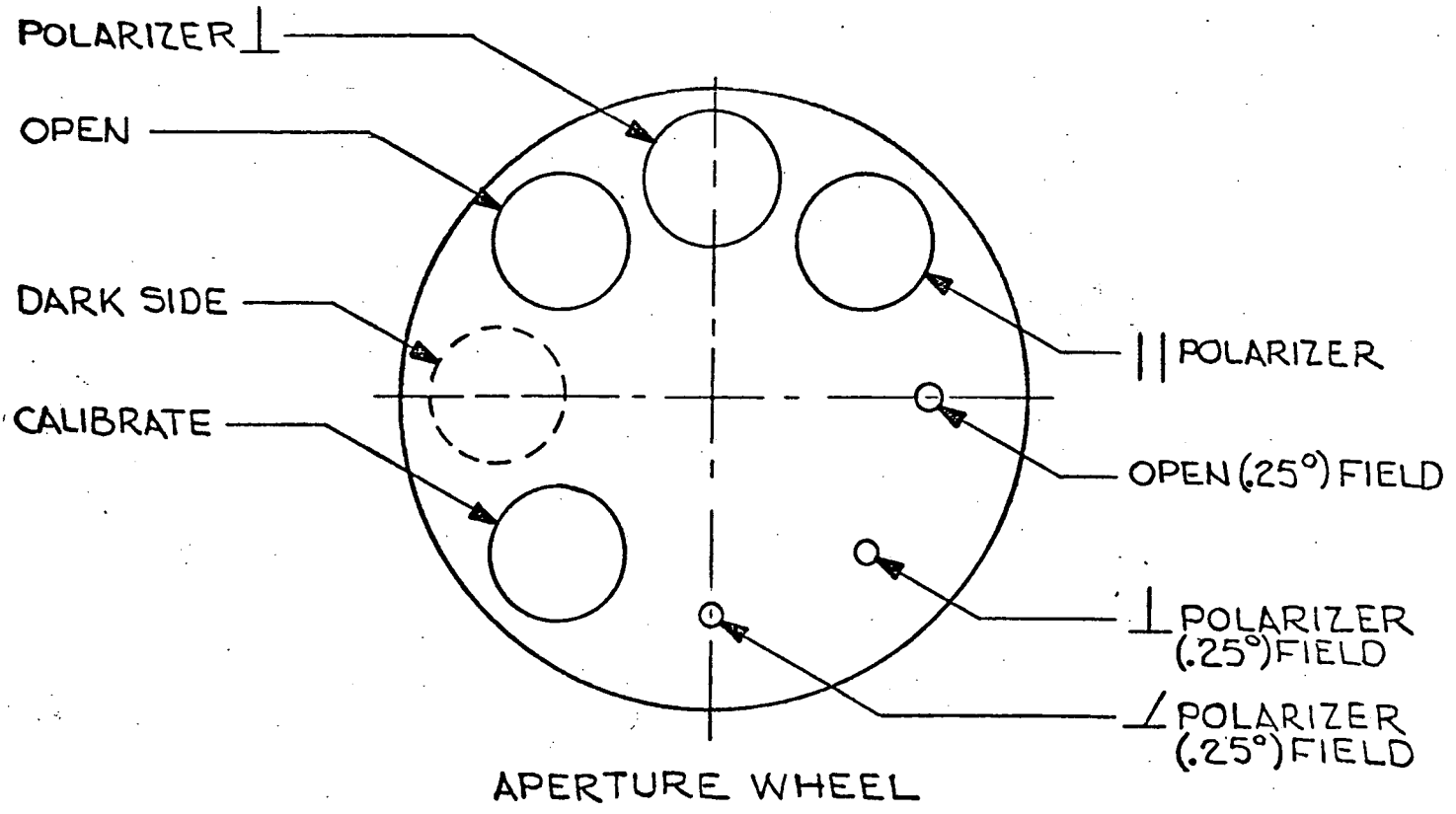

PHOTOPOLARIMETER FOR MJS '77

FIGURE 14

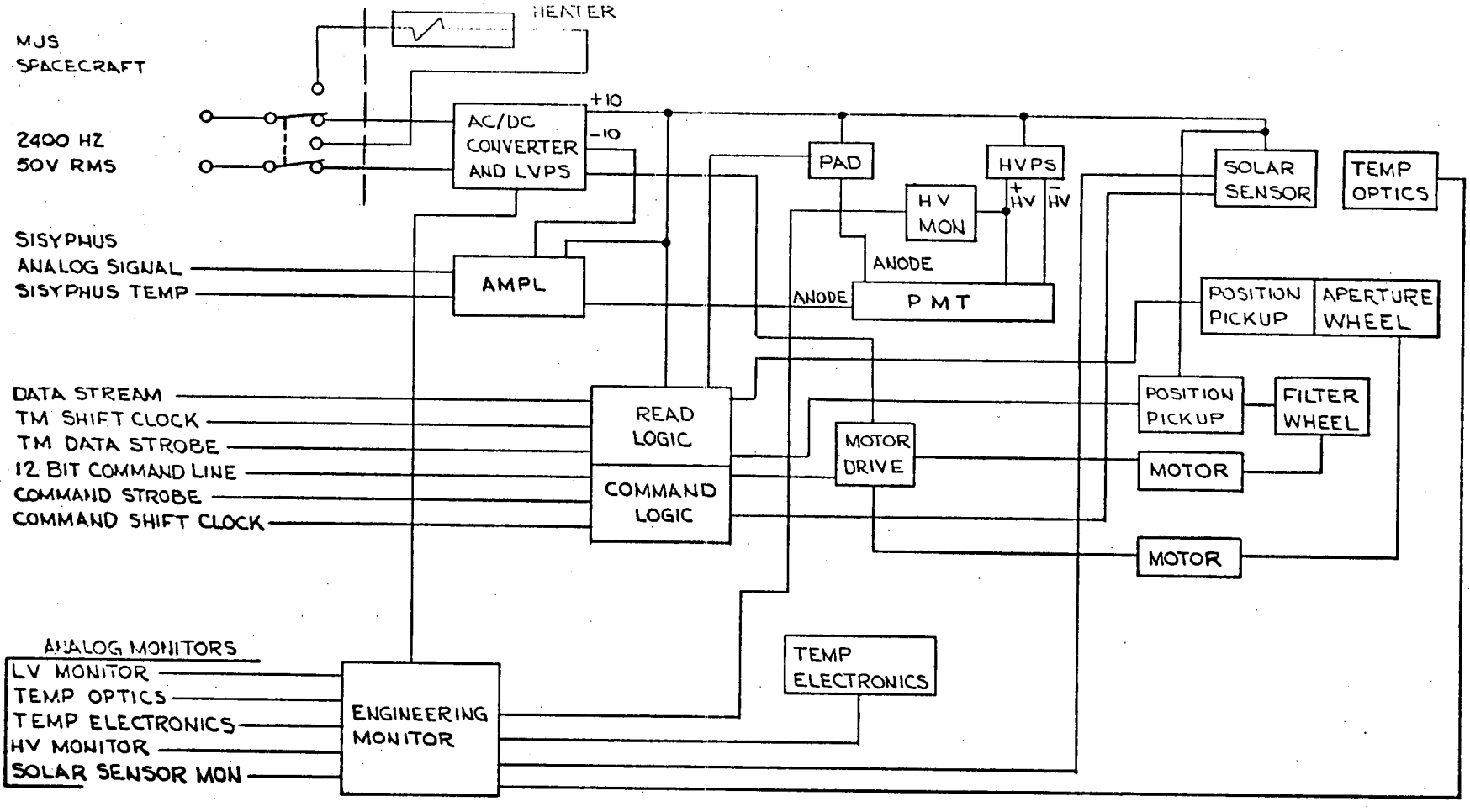

PHOTOPOLARIMETER SYSTEM DESIGN

FIGURE 15

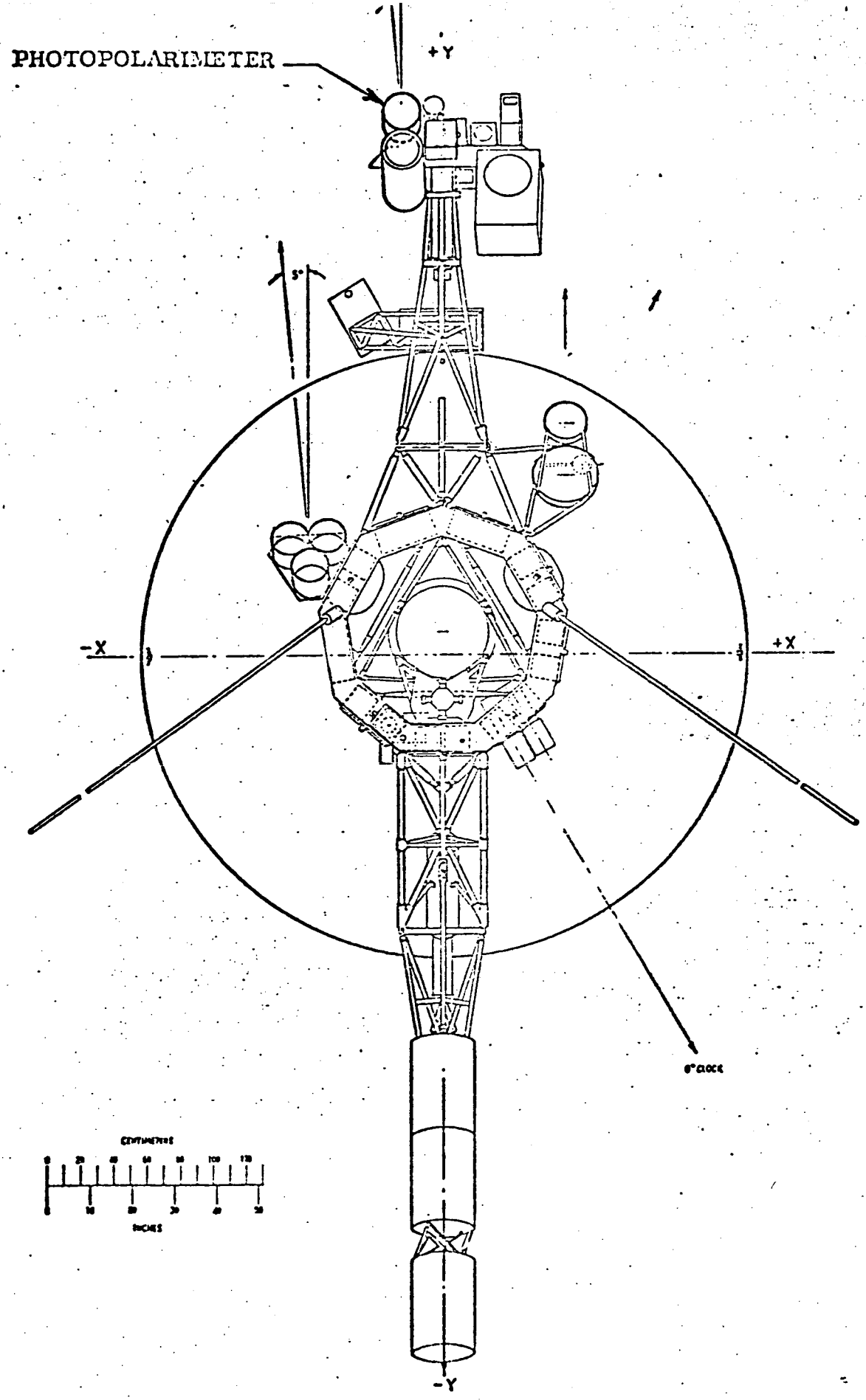

PHOTOPOLARIMETER INSTRUMENTATION ON MJS '77

FIGURE 16

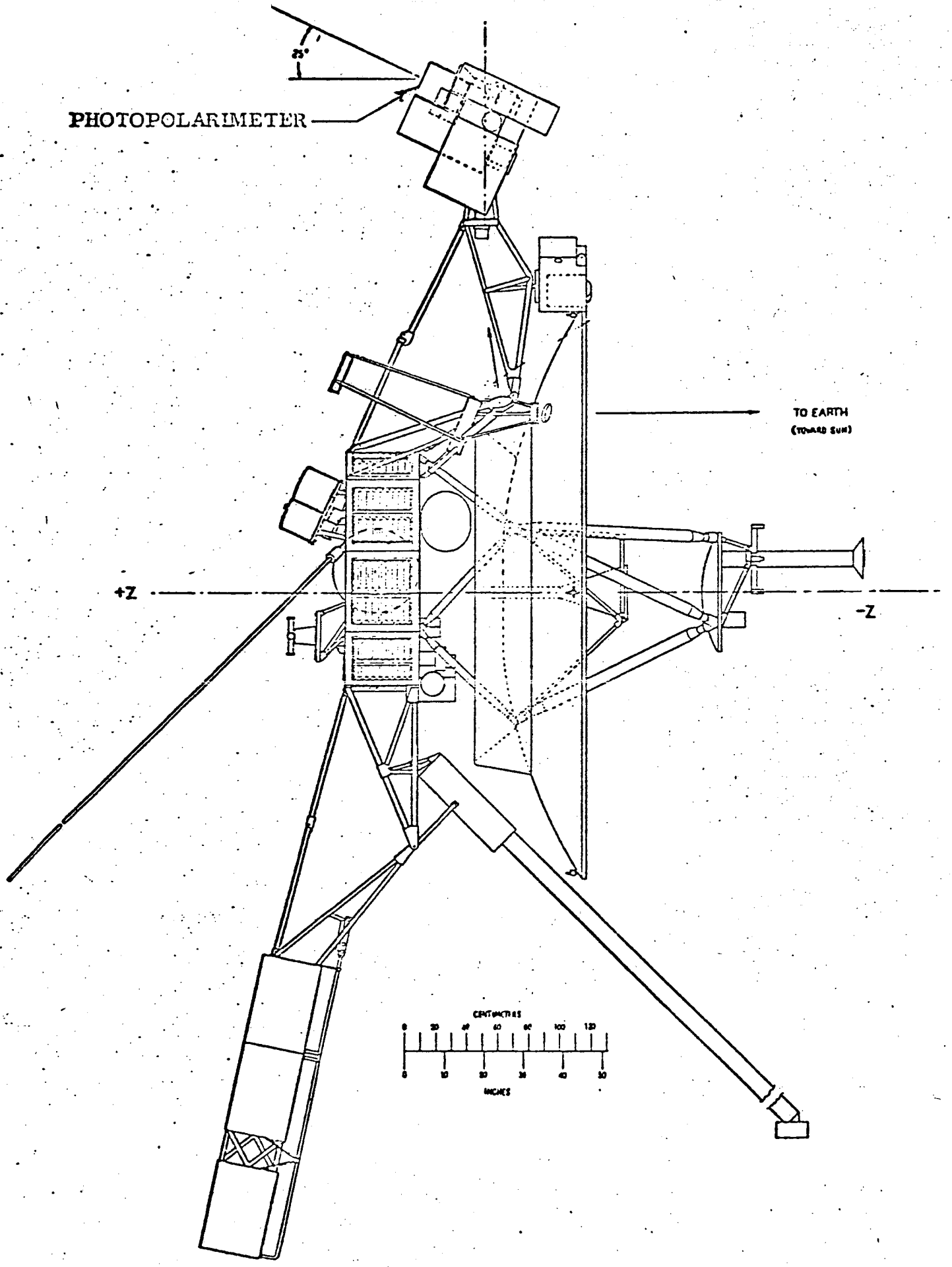

PHOTOPOLARIMETER INSTRUMENTATION ON MJS '77

FIGURE 17